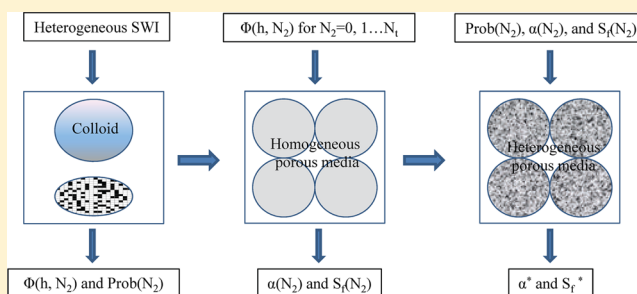


Colloid Adhesive Parameters for Chemically Heterogeneous Porous Media

Scott A. Bradford^{*,†} and Saeed Torkezaban[‡][†]U.S. Salinity Laboratory, USDA, ARS, Riverside, California, United States[‡]Commonwealth Scientific and Industrial Research Organisation (CSIRO) Land and Water, Private Bag 2, Glen Osmond, SA 5064, Australia

ABSTRACT: A simple modeling approach was developed to calculate colloid adhesive parameters for chemically heterogeneous porous media. The area of the zone of electrostatic influence between a colloid and solid–water interface (A_z) was discretized into a number of equally sized grid cells to capture chemical heterogeneity within this region. These cells were divided into fractions having specific zeta potentials (e.g., negative or positive values). Mean colloid adhesive parameters such as the zeta potential, the minimum and maximum in the interaction energy, the colloid sticking efficiency (α), and the fraction of the solid surface area that contributes to colloid immobilization (S_f) were calculated for possible charge realizations within A_z . The probability of a given charge realization in A_z was calculated using a binomial mass distribution. Probability density functions (PDFs) for the colloid adhesive parameters on the heterogeneous surface were subsequently calculated at the representative elementary area (REA) scale for a porous medium. This approach was applied separately to the solid–water interface (SWI) and the colloid, or jointly to both the SWI and colloid. To validate the developed model, the mean and standard deviation of the interaction energy distribution on a chemically heterogeneous SWI were calculated and demonstrated to be consistent with published Monte Carlo simulation output using the computationally intensive grid surface integration technique. Our model results show that the PDFs of colloid adhesive parameters at the REA scale were sensitive to the size of the colloid and the heterogeneity, the charge and number of grid cells, and the ionic strength.



INTRODUCTION

Interaction energies between particles (clays, metal oxides, humic substances, nanoparticles, and microorganisms) and environmental surfaces play a critical role in colloid transport, retention, release, and aggregation that is of great importance in many environmental and industrial processes. The interaction energy of particles with the solid–water interface (SWI) and the stability of particle suspensions is commonly quantified using theory developed by Derjaguin–Landau–Verwey–Overbeek (DLVO).^{1,2} Standard DLVO calculations employ information from measured or estimated zeta potentials of particle suspensions and the SWI that at best reflect only the net electrokinetic properties of the particle and the SWI.³ These DLVO calculations do not account for intrinsic surface microheterogeneity on the SWI and particle that can generate localized regions where the interaction is favorable, even though the medium’s average interaction is unfavorable.^{4,5} Thus, there are more retention sites for negatively charged particles when the SWI is coated with clay particles, which might have patch-wise surface heterogeneities due to isomorphic substitutions, and/or metal oxides.^{4,6–8} Nanoscale heterogeneities have often been implicated in observed attachment under unfavorable conditions.^{9–17}

A variety of surface integration techniques have been developed and utilized to account for the influence of microscopic physical and/or chemical heterogeneity on interaction energies.^{10,11,15,18–21} For example, the grid surface integration (GSI) technique utilizes known solutions for particle interactions between two parallel plates to compute the interaction between a particle and a heterogeneously patterned surface.¹³ The plane and particle surfaces are discretized into small, equally sized, elemental areas to capture desired features on the surfaces. Each elemental area can be assigned a different surface charge and/or Hamaker constant. The GSI technique calculates the total interaction energy on the particle by summing the contribution on each of the discretized surface elements over the entire particle surface.

Some researchers have attempted to explicitly account for the influence of microscopic heterogeneity on colloid transport and retention in trajectory simulations.^{15,22} Determination of the forces and torques that act on colloids in these trajectory simulations requires full knowledge of the flow field, the heterogeneity, repeated surface integration calculations, and

Received: July 24, 2012

Revised: September 7, 2012

Published: September 7, 2012

very small spatial grid sizes and time steps. Although these simulations have provided valuable information on the role of microscopic physical and chemical heterogeneity in colloid transport and retention, limitations also exist. For example, detailed information about the distribution of microscopic heterogeneity is generally not available, so simplified random representations are typically considered. Furthermore, colloid trajectory simulations over heterogeneous surfaces are very computationally intensive. This is especially true when the surface heterogeneity varies temporally with changes in solution chemistry as a result of processes such as protonation/deprotonation of hydroxyl groups, adsorption of different ions, and organics. Consequently, colloid trajectory simulations over heterogeneous surfaces have been limited to the pore-scale and to constant solution chemistry conditions.^{15,22}

Continuum models average heterogeneous flow and transport properties that occur at the pore-scale over a representative elementary volume (REV) or area (REA) to obtain effective lumped parameters. Continuum models are therefore much more computationally efficient than trajectory models, and are commonly employed to simulate colloid transport, retention, and release at larger spatial and temporal scales,^{23–25} and for temporally variable solution chemistry conditions.^{26,27} Colloid adhesive parameters that influence colloid retention and release in a porous medium at the REV scale include the colloid sticking efficiency (α) from filtration theory²⁸ and the maximum solid phase concentration of retained colloids (S_{\max}) in the Langmuirian blocking model.²⁹ In addition, microscopic heterogeneity at the REA scale will produce adhesive parameter values that are not single valued, but rather associated with a probability density function (PDF). Methods to determine the influence of microscopic chemical heterogeneity on the PDF of α and S_{\max} are still lacking. Consequently, continuum models frequently require optimization of adhesive parameters to experimental data.^{26,27}

The overall objective of this research is to overcome some of the outlined limitations by developing a simplified model to account for the influence of microscopic chemical heterogeneity on colloid adhesive parameters for continuum models.

THEORY

Modeling the Influence of Chemical Heterogeneity on the SWI or Colloid. Figure 1 presents a schematic of a homogeneous colloid interacting with a SWI having microscale charge heterogeneities. The interaction energy that the colloid experiences depends

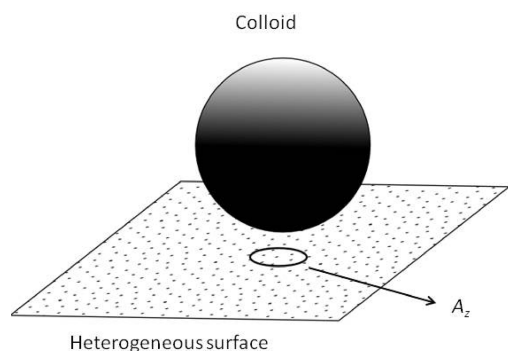


Figure 1. Schematic of a homogeneous colloid interacting with a heterogeneously charged SWI. The area of the zone of electrostatic influence (A_z) depends on the colloid size and the double layer thickness.

on its spatial location and distance from the SWI. However, only a small portion of the SWI contributes to the interaction energy at any particular location and this is referred to as the zone of electrostatic influence.¹⁵ The area of the zone of electrostatic influence (A_z , L^2) depends on the colloid size and the double layer thickness as¹⁵

$$A_z \cong \frac{4\pi r_c}{\kappa} \quad (1)$$

where r_c [L] is the colloid radius and κ [L^{-1}] is the Debye–Huckel parameter. Note that the surface charge can be heterogeneously distributed within A_z . The value of A_z can be therefore discretized into a number of equally sized cells to account for this charge heterogeneity. The total number of cells (N_t) is determined by the ratio of A_z to the area of the heterogeneity size (A_h , L^2). Each cell is associated with a zeta potential (and/or Hamaker constant) of type 1 (e.g., negative zeta potential value) or type 2 (e.g., positive or less negative zeta potential).

As the colloid moves along the microscopically heterogeneous surface different numbers of type 1 and 2 cells occur within A_z . Each spatial location on the SWI constitutes a realization of the microscopic heterogeneity. The mean zeta potential within A_z (ζ , mV) is easily determined as

$$\zeta = \left(1 - \frac{N_2}{N_t}\right)\zeta_1 + \frac{N_2}{N_t}\zeta_2 \quad (2)$$

where N_2 is the number of cells associated with type 2, and ζ_1 (mV) and ζ_2 (mV) are the zeta potentials associated with types 1 and 2, respectively. Bendersky and Davis²¹ found that GSI results for the mean dimensionless (divided by the product of the Boltzmann constant, k_B , and the absolute temperature, T_K) interaction energy (Φ) on heterogeneous surfaces were not consistent with the use of mean values of ζ because of the nonlinear dependence of Φ on ζ . However, these authors found that a linear combination of the dimensionless interaction energies associated with type 1 (Φ_1) and type 2 (Φ_2) cells provided good agreement with GSI results. The mean value of Φ within A_z is therefore determined as

$$\Phi(h) = \left(1 - \frac{N_2}{N_t}\right)\Phi_1(h) + \frac{N_2}{N_t}\Phi_2(h) \quad (3)$$

where h is the separation distance. Values of Φ_1 and Φ_2 were calculated using DLVO theory and a sphere-plate assumption.^{1,2} Electrostatic double layer interactions were quantified using the expression of Hogg et al.³⁰ using ζ_1 and ζ_2 in place of surface potentials. The retarded London–van der Waals attractive interaction force was determined from the expression of Gregory.³¹

Mean values of ζ , $\Phi(h)$, the energy barrier height (Φ_{\max}), and the depth of the secondary minimum ($\Phi_{2\min}$) were calculated for possible charge distribution realizations ($N_2 = 0, 1, \dots, N_t$) within A_z using eqs 2 and 3. The particular location of the type 2 cells within A_z was not needed to determine these statistically mean values.²¹ Conditions are unfavorable for attachment within A_z when $\Phi_{\max} > 0$ and favorable when $\Phi_{\max} = 0$. The value of $\Phi_{2\min}$ may be greater than zero under unfavorable conditions, but $\Phi_{2\min} = 0$ under favorable conditions. DLVO theory assumes that the depth of the primary minimum ($\Phi_{1\min}$) is infinite. However, it may be possible to include non-DLVO interactions (e.g., Born repulsion) in eq 3 to produce a finite value of $\Phi_{1\min}$.

Equation 3 indicates that attachment conditions will depend on the values of N_2 and $N_t = A_z/A_h$, as well as properties that influence Φ_1 and Φ_2 . When the left-hand side of eq 3 is set equal to zero the critical value of N_2 to achieve favorable attachment conditions ($N_{2\text{crit}}$) can be determined as:

$$N_{2\text{crit}} = \frac{N_t C_\Phi}{1 + C_\Phi} \quad (4)$$

where C_Φ is a constant given as:

$$C_\Phi = -\frac{\Phi_1(h_{\max})}{\Phi_2(h_{\max})} \quad (5)$$

and h_{\max} is the distance that corresponds to Φ_{\max} . Favorable attachment conditions ($\Phi_{\max} = 0$) occur within A_z when $N_2 \geq N_{2\text{crit}}$, whereas conditions are unfavorable ($\Phi_{\max} > 0$) when $N_2 < N_{2\text{crit}}$. However, only truncated values of $N_{2\text{crit}}$ contribute to the number of favorable categories in the PDF because N_2 is an integer.

Calculated values of $\Phi_{2\text{min}}$ or $\Phi_{1\text{min}}$ (Φ_{min}) within A_z are used to determine the corresponding resisting (adhesive) torque (T_{adhesion} , ML^2T^{-2} where M , L , and T denote units of mass, length, and time, respectively). The value of $T_{\text{adhesion}} = l_x F_A$, where l_x (L) is the lever arm and F_A ($M L T^{-2}$) is the pull-off adhesive force that is required to mobilize a colloid from Φ_{min} .³² Derjaguin and Langbein approximations may be used to estimate F_A as $(\Phi_{\text{min}} k_B T_K)/h$.^{33,34} Some researchers have assumed an empirical value of l_x to account for friction arising from surface roughness and/or chemical heterogeneity.^{15,35} Alternatively, theory by Johnson, Kendall, and Roberts (JKR) may be used to estimate l_x as a result of resistance due to deformation at separation^{36,37} for colloid attachment under favorable or unfavorable conditions.^{34,38–42} We have therefore chosen to estimate l_x from the JKR model. Additional details about the determination of T_{adhesion} are available in the literature.^{39,42}

The fraction of the solid surface area that contributes to colloid immobilization (S_f) can be linearly related to S_{max} .⁴³ Values of S_f were determined by considering the effects of the velocity distribution at the SWI in a homogeneous porous medium with $\Phi(h)$ equivalent to a charge heterogeneity realization. The value of S_f was determined from a torque balance by evaluating the log-normal cumulative density function (CDF) of applied hydrodynamic torque (T_{applied} , ML^2T^{-2}) at T_{adhesion} as:⁴²

$$S_f = \frac{1}{2} + \frac{1}{2} \text{erf}\left(\frac{\ln(T_{\text{adhesion}}) - \mu}{\sigma\sqrt{2}}\right) \quad (6)$$

where μ and σ are the mean and variance of the log-normal CDF of T_{applied} . The value of μ for the log-normal distribution is defined as:

$$\mu = \ln(T_{50}) \quad (7)$$

Here T_{50} [ML^2T^{-2}] corresponds to the median value of T_{applied} on the SWI. Bradford et al.⁴² presented a detailed approach to predict the CDF of T_{applied} on packs of smooth, spherical collectors for different velocities, collector sizes and colloid sizes. The value of T_{applied} varies spatially within a porous medium due to differences in the pore space geometry. Consequently, only a fraction of the SWI may contribute to colloid immobilization for a given value of T_{adhesion} . On heterogeneous surfaces the value of S_f can be divided into contributions from a primary (S_{f1}) and secondary (S_{f2}) minimum as $S_f = S_{f1} + S_{f2}$. When $\Phi_{\max} = 0$ the value of $S_{f1} = 1$ (or eq 6) and $S_{f2} = 0$. Conversely, when $\Phi_{\max} > 0$, the value of $S_{f1} = 0$ and S_{f2} is determined by eq 6.

Values of α were determined to predict the effects of colloid diffusion in a homogeneous porous medium with $\Phi(h)$ equivalent to a charge heterogeneity realization. The kinetic energy method^{44–46} estimates the fraction of colloids that will diffuse over the energy barrier (α_1) and the fraction that will interact with the secondary minimum (α_2) based on the kinetic energy distribution of diffusing colloids as

$$\alpha_1 = 1 - \left(\text{erf}(\sqrt{\Delta\Phi}) - \sqrt{\frac{4\Delta\Phi}{\pi}} \exp(-\Delta\Phi) \right) \quad (8)$$

$$\alpha_2 = \text{erf}(\sqrt{\Phi_{2\text{min}}}) - \sqrt{\frac{4\Phi_{2\text{min}}}{\pi}} \exp(-\Phi_{2\text{min}}) \quad (9)$$

where $\Delta\Phi = \Phi_{2\text{min}} + \Phi_{\max}$. The total value of $\alpha = \alpha_1 + \alpha_2$. When $\Phi_{\max} = 0$ the value of $\Phi_{2\text{min}} = 0$, $\alpha_1 = 1$, and $\alpha_2 = 0$.

The above information describes the determination of mean values of ζ , $\Phi_{2\text{min}}$, and Φ_{\max} for possible charge heterogeneity realizations ($N_2 = 0, 1, \dots, N_t$) within A_z . This information was subsequently used to estimate α and S_f in homogeneous porous media having $\Phi(h)$

equivalent to these same charge heterogeneity realizations. Additional information is needed to determine the PDFs for these adhesive parameters on a chemically heterogeneous porous medium at the REA scale. If the total fraction of type 2 sites is known on the SWI at the REA scale of a porous medium (P_s) and the charge heterogeneity is randomly distributed as shown in Figure 1, then the probability for the occurrence for each charge realization ($\text{Prob}(N_2)$) within A_z is obtained from the binomial mass distribution as:

$$\text{Prob}(N_2) = \frac{N_t!}{N_2!(N_t - N_2)!} P_s^{N_2} (1 - P_s)^{N_t - N_2} \quad (10)$$

The associated PDF for $\zeta(N_2)$, $\Phi_{2\text{min}}(N_2)$, $\Phi_{\max}(N_2)$, $\alpha(N_2)$, and $S_f(N_2)$ at the REA scale of a porous medium are obtained by plotting versus $\text{Prob}(N_2)$. It follows that the mean value of ζ on the entire heterogeneous surface at the REA scale is given as

$$\zeta^* = \langle \zeta \rangle = \sum_{N_2=0}^{N_t} \text{Prob}(N_2) \zeta(N_2) \quad (11)$$

Here the superscript * is used to denote the mean value of a given parameter at the REA scale. The variance of ζ is given as $\langle \zeta^2 \rangle - \langle \zeta \rangle^2$, and the associated standard deviation is equal to the square root of the variance.⁴⁷ Similar expressions were used to determine the mean, variance, and standard deviation of $\Phi_{2\text{min}}$, Φ_{\max} , α , α_1 , α_2 , S_{f1} , and S_{f2} at the REA scale by replacing ζ^* and ζ terms in eq 11.

The above approach assumed no charge heterogeneity on the colloid surface. When the surface charge of the SWI is uniform, a similar approach may be applied to a heterogeneously charged colloid population by simply reversing the roles of the SWI and colloid. In this case, each colloid that approaches the solid surface constitutes a realization of the charge heterogeneity. The charge heterogeneity of the colloid population is again quantified by the binomial distribution.

Modeling the Influence of Chemical Heterogeneity on the SWI and the Colloid. This model may be further extended to include the influence of a heterogeneously charged colloid and SWI after making several assumptions. As a first approximation, we select A_z to be the same value (eq 1) for both the SWI (cf. Figure 1) and colloid. This implies symmetry in the electrostatic zone of influence on the SWI and colloid. Similar to GSI calculations, a value of A_h is chosen to reflect the smallest sized heterogeneity of interest on either the SWI or colloid. The determination of the mean value of $\Phi(h)$ within A_z is now a linear combination of four values of Φ (instead of two in eq 3) as

$$\Phi(h) = f_{11} \Phi_{11}(h) + f_{12} \Phi_{12}(h) + f_{21} \Phi_{21}(h) + f_{22} \Phi_{22}(h) \quad (12)$$

Here Φ_{11} , Φ_{12} , Φ_{21} , and Φ_{22} denote the interaction energy between type 1 and/or 2 cells on the colloid and SWI. The values of f_{11} , f_{12} , f_{21} , and f_{22} reflect the fractions of type 1 and 2 cells on the colloid and SWI as

$$f_{11} = \left(1 - \frac{N_2^c}{N_t}\right) \left(1 - \frac{N_2^s}{N_t}\right) \quad (13)$$

$$f_{21} = \frac{N_2^c}{N_t} \left(1 - \frac{N_2^s}{N_t}\right) \quad (14)$$

$$f_{12} = \left(1 - \frac{N_2^c}{N_t}\right) \frac{N_2^s}{N_t} \quad (15)$$

$$f_{22} = \frac{N_2^c}{N_t} \frac{N_2^s}{N_t} \quad (16)$$

where N_2^c and N_2^s are the number of type 2 sites in A_z on the SWI and colloid, respectively.

Mean values of $\Phi(h)$ within A_z were calculated for possible charge distribution realizations using eq 12, and $\Phi_{2\text{min}}$, Φ_{\max} , α , α_1 , α_2 , S_{f1} , and S_{f2} were determined using the same procedures described above. However, the total number of realizations of charge heterogeneity on both the SWI and colloid is now equal to N_t^2 .

The probability for occurrence for each charge realization on the SWI and the colloid at the REA scale is given by the joint binomial mass distribution as

$$\text{Prob}(N_2^s, N_2^c) = \left(\frac{N_t!}{N_2^s!(N_t - N_2^s)!} P_s^{N_2^s} (1 - P_s)^{N_t - N_2^s} \right) \left(\frac{N_t!}{N_2^c!(N_t - N_2^c)!} P_c^{N_2^c} (1 - P_c)^{N_t - N_2^c} \right) \quad (17)$$

where P_c is the total fraction of type 2 sites on the colloid at the REA scale. Equation 17 assumes that the charge heterogeneity on the colloid and SWI act independently from each other.

The associated probability density functions for $\Phi_{2\min}(N_2^s, N_2^c)$, $\Phi_{\max}(N_2^s, N_2^c)$, $\alpha(N_2^s, N_2^c)$, $\alpha_1(N_2^s, N_2^c)$, $\alpha_2(N_2^s, N_2^c)$, $S_f(N_2^s, N_2^c)$, $S_{f1}(N_2^s, N_2^c)$ and $S_{f2}(N_2^s, N_2^c)$ at the REA scale are obtained by plotting versus $\text{Prob}(N_2^s, N_2^c)$. It follows that the mean value of $\Phi_{2\min}$ on the entire heterogeneous SWI and colloid surface at the REA scale, $\langle \Phi_{2\min} \rangle$, is given as

$$\Phi_{2\min}^* = \langle \Phi_{2\min} \rangle = \sum_{N_2^s=0}^{N_t} \sum_{N_2^c=0}^{N_t} \text{Prob}(N_2^s, N_2^c) \Phi_{2\min}(N_2^s, N_2^c) \quad (18)$$

The variance of $\Phi_{2\min}$ is again given as $\langle \Phi_{2\min}^2 \rangle - \langle \Phi_{2\min} \rangle^2$, and the associated standard deviation is equal to the square root of the variance.⁴⁷ Similar expressions were used to determine the mean, variance, and standard deviation of Φ_{\max} , α , α_1 , α_2 , S_p , S_{f1} , and S_{f2} at the REA scale by replacing the $\Phi_{2\min}$ and $\Phi_{2\min}^*$ terms in eq 18.

RESULTS AND DISCUSSION

Model Validation. Bendersky and Davis²¹ conducted multiple GSI simulations (~200) on a randomly generated chemically heterogeneous SWI. Specific parameter values used in these GSI simulations included $\zeta_1 = -27$ mV, $\zeta_2 = 54$ mV, IS = 5.8 mM ($\kappa^{-1} = 4$ nm), $r_c = 500$ nm, $A_z = 25\,133$ nm², $A_h = 78.5$ nm², and $P_s = 0.196$. The zeta potential of the colloid was -27 mV, and the Hamaker constant equaled 5×10^{-21} J. Figure 2 presents our simulation model output for Φ^* as a function of dimensionless distance (κh) using equivalent properties for the chemically heterogeneous SWI. The error bars in this figure represent ± 1.5 standard deviations. The value of $\Phi_{\max}^* = 42.2$ and $\Phi_{2\min}^* = 0.5$ in Figure 2. The mean values and error bars

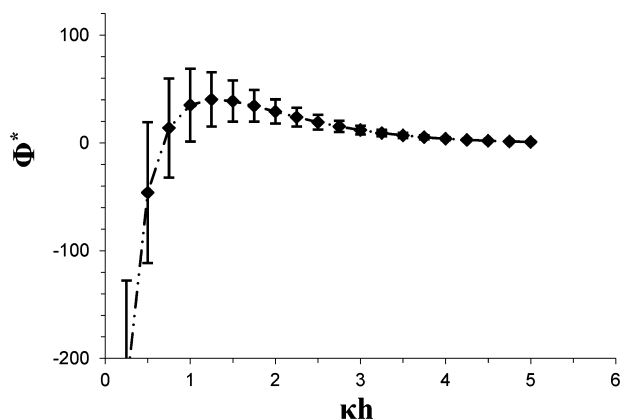


Figure 2. Simulated mean values of Φ^* as a function of dimensionless distance (κh) on a chemically heterogeneous solid-water interface. The error bars in this figure represent ± 1.5 standard deviations. Model parameter values used in this simulations included $\zeta_1 = -27$ mV, $\zeta_2 = 54$ mV, IS = 5.8 mM, $r_c = 500$ nm, $A_z = 25\,133$ nm², $A_h = 78.5$ nm², and $P_s = 0.196$. The zeta potential of the colloid was -27 mV, and the Hamaker constant equaled 5×10^{-21} J.

shown in Figure 2 are nearly identical to that reported by Bendersky and Davis,²¹ providing a validation of our simplified modeling approach on a chemically heterogeneous SWI.

Chemical Heterogeneity on the SWI. Numerical experiments were conducted to investigate the influence of chemical heterogeneity on colloid adhesive parameters. Unless otherwise noted all of the simulations considered below used a value of Darcy water velocity of 0.1 cm min⁻¹, a porosity of 0.34, a median grain size of 360 μ m, a colloid zeta potential of -30 mV, and a Hamaker constant of 4.04×10^{-21} J.

The value of S_{f1}^* at the REA scale of a porous medium (eq 11) is controlled by the number of favorable categories in the PDF which occur when $N_2 \geq N_{2\text{crit}}$ (eq 4), and the probability of occurrence of these categories which is determined by eq 10. Figure 3 presents values of S_{f1}^* as a function of ζ_2 when $\zeta_1 =$

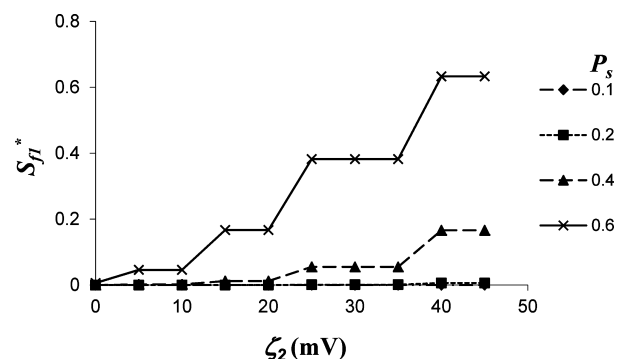


Figure 3. Values of S_{f1}^* as a function of ζ_2 for a homogeneously charged colloid (-30 mV) on various heterogeneously charged porous media. Simulation properties included the following: $\zeta_1 = -70$ mV, IS = 10 mM, $r_c = 500$ nm, $N_t = A_z/A_h = 10$, a Hamaker constant of 4.04×10^{-21} J, and $P_s = 0.1, 0.2, 0.4,$ and 0.6 .

-70 mV, IS = 10 mM, $r_c = 500$ nm, $N_t = A_z/A_h = 10$ and $P_s = 0.1, 0.2, 0.4,$ and 0.6 . The value of ζ_2 has a strong influence on $N_{2\text{crit}}$ (eq 4), and thereby influences the number of categories in the PDF that are favorable for attachment ($N_t - N_{2\text{crit}}$). Step changes in S_{f1}^* with ζ_2 are due to the presence of incremental increases in ($N_t - N_{2\text{crit}}$) after exceeding a value of ζ_2 that induces a reduction in the truncated value of $N_{2\text{crit}}$. The value of P_s determines the probability of occurrence of the favorable categories in eq 10. Consequently, the value of S_{f1}^* increases with P_s for a given ζ_2 . Figure 3 implies that changes in solution chemistry that influence P_s and ζ_2 (e.g., cation exchange and pH variations) are expected to influence S_{f1}^* .

In addition to P_s and ζ_2 , the values of $\text{Prob}(N_2)$ (eq 10) and $N_{2\text{crit}}$ (eq 4) are also functions of $N_t = A_z/A_h$. It is worthwhile to mention that N_t is directly related to the colloid radius and inversely related to the solution IS as is evident in eq 1. Figure 4 presents values of S_{f1}^* as a function of N_t when $\zeta_1 = -70$ mV, $\zeta_2 = 0$ mV, and $P_s = 0.1, 0.2, 0.4,$ and 0.6 . The value of S_{f1}^* is strongly dependent on N_t , and rapidly decreases as N_t increases. The value of S_{f1}^* increases with P_s at a given value of N_t , and $S_{f1}^* = P_s$ when $N_t = 1$. These trends can be explained by the probability of the occurrence of favorable categories in the PDF which decreases with N_t and increases with P_s (eq 10). In Figure 4 the value of ($N_t - N_{2\text{crit}}$) = 1. More complex behavior is obtained at higher ζ_2 when ($N_t - N_{2\text{crit}}$) changes with N_t (similar to Figure 3). In general, increasing ζ_2 at a given N_t produces higher values of S_{f1}^* because of its influence on $N_{2\text{crit}}$ (eq 4).

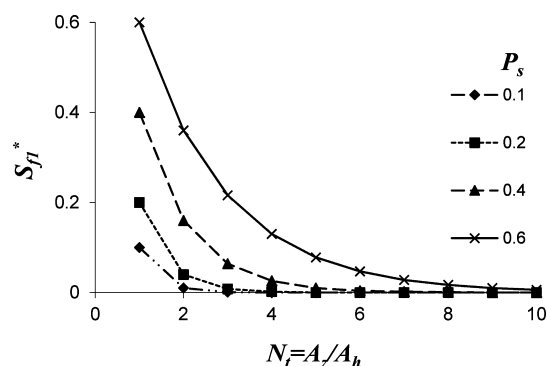


Figure 4. Values of S_{fi}^* as a function of N_t for a homogeneously charged colloid (-30 mV) on various heterogeneously charged porous media. Simulation properties included the following: $\zeta_1 = -70$ mV, $\zeta_2 = 0$ mV, a Hamaker constant of 4.04×10^{-21} J, and $P_s = 0.1, 0.2, 0.4,$ and 0.6 .

Figure 5 presents values of S_{fi}^* as a function of r_c when $A_h = 2500$ nm², $\zeta_1 = -70$ mV, $\zeta_2 = 20$ mV, $P_s = 0.1$, and IS = 2, 25,

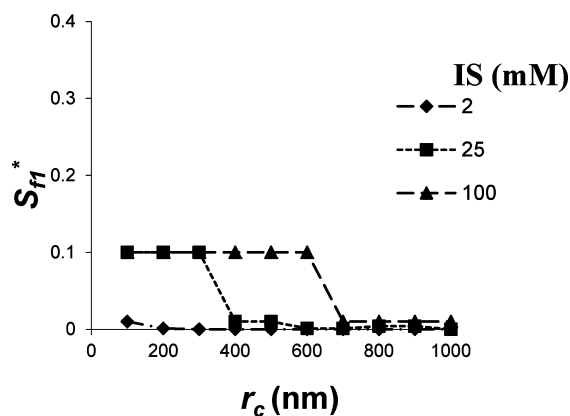


Figure 5. Values of S_{fi}^* as a function of r_c for a homogeneously charged colloid (-30 mV) on various heterogeneously charged porous media. Simulation properties including the following: $A_h = 2500$ nm², $\zeta_1 = -70$ mV, $\zeta_2 = 20$ mV, $P_s = 0.1$, a Hamaker constant of 4.04×10^{-21} J, and IS = 2, 25, and 100 mM.

and 100 mM. Simulated values of S_{fi}^* increased with decreasing r_c and increasing IS. Consequently, one important conclusion is that a given sized chemical heterogeneity will produce larger values of S_{fi}^* for smaller colloids and higher IS. These trends have been experimentally observed,²⁷ and can be explained by the observed dependency of S_{fi}^* on $N_t = A_z/A_h$ (Figure 4). In particular, eq 1 indicates that values of N_t decrease for smaller r_c and higher IS. Similar to the Figure 4, values of S_{fi}^* therefore increase with decreasing N_t (smaller r_c and higher IS) due to an associated increase in the probability of favorable categories in the PDF (eq 10). Interaction in the primary minimum is expected to be independent of the solution IS when $N_t < 1$.⁴⁸ However, attachment in the primary minimum may change with solution IS when $N_t > 1$.⁴⁹ Results shown in Figures 4 and 5 predict these trends.

The value of α_1^* was typically equal to S_{fi}^* as has been experimentally observed by Elimelech et al.⁵⁰ This indicates that α_1^* was controlled by the presence of favorable regions and that there was a significant energy barrier in unfavorable regions. Consequently, α_1^* exhibited the same dependency as S_{fi}^* on P_s , ζ_2 , $N_t = A_z/A_h$, IS, and r_c shown in Figures 3–5 and

discussed above. Note that this prediction is consistent with conventional filtration theory²⁸ that assumes colloid immobilization occurs instantaneously with collision on the SWI. However, values of $\alpha^* \gg S_f^*$ have been reported in the literature for unfavorable attachment conditions.^{49,51} This condition implies that colloid immobilization is not instantaneous on the SWI. Rather, colloids may interact with a porous medium by a secondary minimum in unfavorable locations, and become immobilized or roll on the SWI depending on the local balance of applied hydrodynamic and resisting adhesive torques. Rolling colloids may subsequently detach from the SWI or encounter regions that are chemically and/or hydrodynamically favorable for retention.^{40,42,52}

Calculated colloid adhesive parameters for chemically heterogeneous porous media provide additional insight on the importance of rolling and the secondary minimum on colloid retention. Similar to eq 2, the value of ζ^{r*} changed in a linear fashion with P_s , ζ_1 , and ζ_2 . This trend has been experimentally verified and is consistent with the mean properties of the SWI.^{50,53} Increasing ζ^* (less negative) occurs with increasing P_s and/or ζ_2 . DLVO theory predicts that Φ_{2min}^* increases with ζ^* , IS, r_c , and Hamaker constant. Below we demonstrate that the value of Φ_{2min}^* can have a strong influence on predicted values of α^* and S_f^* .

Figure 6 shows predicted values of α^* (Figure 6a) and S_f^* (Figure 6b) with IS for $A_h = 500$ nm², $\zeta_1 = -70$ mV, $\zeta_2 = 20$ mV, $P_s = 0.1$, and $r_c = 5000, 2500, 1250, 500,$ and 250 nm. In this example, the value of $\alpha^* = \alpha_2^*$ and $S_f^* = S_{f2}^*$ because $\alpha_1^* = S_{f1}^* = 0$.

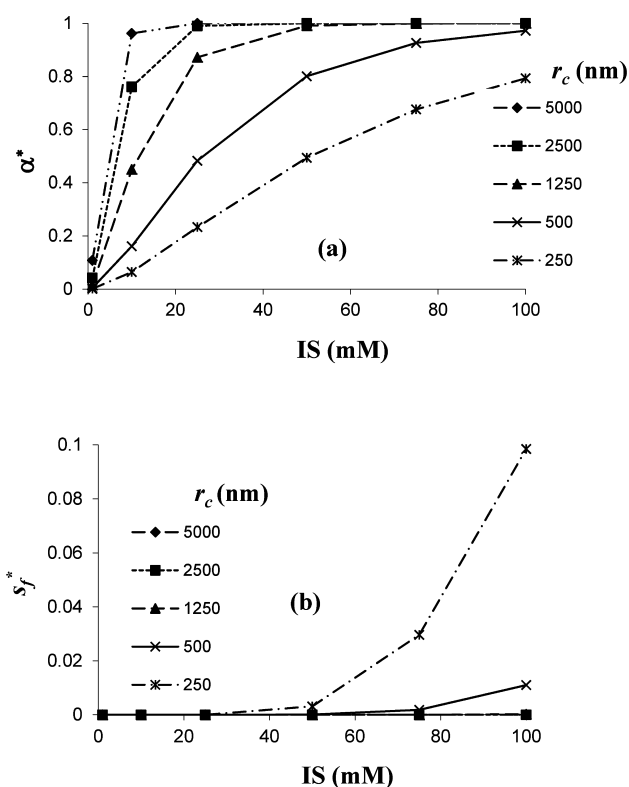


Figure 6. Predicted values of α^* (a) and S_f^* (b) as a function of IS for a homogeneous colloid (-30 mV) on a heterogeneous porous medium. Simulation properties included $A_h = 500$ nm², $\zeta_1 = -70$ mV, $\zeta_2 = 20$ mV, $P_s = 0.1$, a Hamaker constant of 4.04×10^{-21} J, and $r_c = 5000, 2500, 1250, 500,$ and 250 nm. In this example, the value of $\alpha^* = \alpha_2^*$ and $S_f^* = S_{f2}^*$ because $\alpha_1^* = S_{f1}^* = 0$.

$= S_{f1}^* = 0$. Similar to Φ_{2min}^* , the value of α^* rapidly increases with IS and r_c . In contrast, the value of S_f^* only increases with IS as r_c decreases. The value of S_{f2}^* depends on the balance of $T_{applied}$ and $T_{adhesion}$ according to eq 6. Both $T_{applied}$ and $T_{adhesion}$ are functions of r_c ³⁹ but $T_{applied}$ decreases more rapidly (proportional to r_c^3) than $T_{adhesion}$ with r_c . Consequently, S_f^* is larger for smaller r_c even though Φ_{2min}^* is also smaller. This prediction is supported by the observation that α^* was around 50 times greater than S_f^* for nanoparticles.^{49,51} The predicted trends for α_1^* and S_{f1}^* were already discussed above (Figures 4 and 5). Based on this information, the values of α_2^* and S_{f2}^* are expected to dominate the determination of α^* and S_f^* , respectively, at higher values of $N_t = A_z/A_h$ and for smaller values of P_s and ζ_2 .

It should be mentioned that the value of $N_t = A_z/A_h$ increases with smaller A_h , larger colloids, and lower IS. All of these factors will directly influence Φ_{2min}^* and thus the determination of α_2^* . Experimental values of α^* have also been reported to decrease with increasing water velocity.^{41,54} Shen et al.⁴¹ accounted for this velocity dependency by multiplying α_1^* and α_2^* by S_{f1}^* and S_{f2}^* , respectively. It is clear from the above results that S_{f2}^* is strongly influenced by the system hydrodynamics (increasing with decreasing r_c). It is interesting to note that S_f^* was frequently found to be zero for larger colloids ($>1 \mu\text{m}$). This suggests the importance of other factors in controlling the immobilization of larger colloids that were not fully accounted for in the torque balance calculations. For example, microscopic observations and theoretical calculations demonstrate the importance of surface roughness comparable in size to the colloid and grain–grain contacts on colloid immobilization in porous media under unfavorable attachment conditions.^{55–58} These physical factors will influence the calculation of applied and resisting torques that act on colloids near the SWI.^{59,60} In addition, eddy zones have also been demonstrated to contribute to colloid retention in porous media.^{40,61,62}

Hysteresis in S_f^* with IS has been reported in the literature.^{27,63,64} The above results indicate that this is likely due to the different dependence of S_{f1}^* and S_{f2}^* on IS. In particular, colloids immobilized within a secondary minimum, S_{f2}^* , are expected to be reversibly retained because Φ_{2min}^* decreases with a reduction in IS. In contrast, colloid release from a primary minimum, S_{f1}^* , depends on the difference in the depth of the primary minimum and the height of the energy barrier, and this difference needs to be less than a few $k_B T_K$ for colloids to escape the SWI via diffusion and/or hydrodynamic forces. Non-DLVO forces, such as Born repulsion, need to be considered in interaction energy calculations to achieve a finite depth of the primary minimum that changes with IS. However, an increase in Φ_{max}^* is actually predicted with a reduction in solution IS. Colloids in a primary minimum are therefore expected to be largely irreversible with a reduction in IS. However, it should be mentioned that colloid release from a primary minimum has been observed with cation exchange when divalent cations are replaced by monovalent cations.^{65,66} In this case, it is likely that cation exchange is actually altering the chemical heterogeneity on the SWI to eliminate some primary minimum interactions by reducing P_s and/or ζ_2 . Additional research is needed to fully resolve this issue.

Chemical Heterogeneity on Colloids and SWI. The above simulations considered only chemical heterogeneity on the SWI. Simulations shown in Figures 4 and 6 were rerun for the case of chemical heterogeneity on both the SWI and the

colloid. Parameter values for the SWI were the same as in Figures 4 and 6. In contrast, heterogeneous colloid properties were selected to be $\zeta_1 = -70 \text{ mV}$, $\zeta_2 = 0 \text{ mV}$, and $P_c = 0.57$ to yield a mean ζ for the colloid equal to -30 mV to be consistent with Figures 4 and 6.

Figure 7 presents values of S_{f1}^* at the REA scale as a function of $N_t = A_z/A_h$ for the chemically heterogeneous colloids and

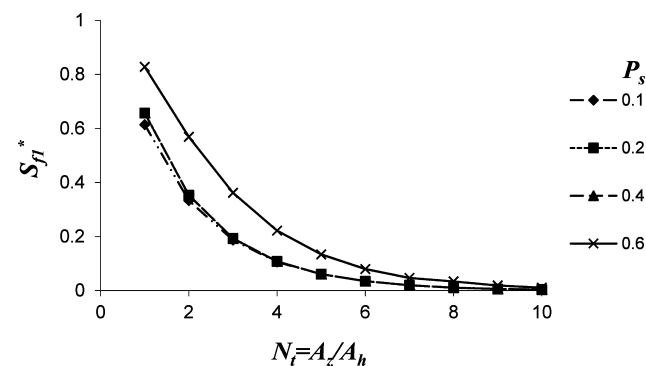


Figure 7. Values of S_{f1}^* as a function of N_t for heterogeneous charged colloids and porous media. Simulation properties included the following: $\zeta_1 = -70 \text{ mV}$ and $\zeta_2 = 0 \text{ mV}$ for both the colloid and the SWI, a Hamaker constant of $4.04 \times 10^{-21} \text{ J}$, $P_c = 0.57$ to yield a mean ζ for the colloid equal to -30 mV to be consistent with Figure 4, and $P_s = 0.1, 0.2, 0.4,$ and 0.6 .

SWI. The value of S_{f1}^* tended to be larger in Figure 7 than Figure 4 especially for lower values of P_s , indicating that S_{f1}^* was strongly influenced by heterogeneity on both the SWI and the colloid. In this case, S_{f1}^* was determined by the probability of occurrence of high values of N_1^z and/or N_2^z that depended on P_s and P_c , respectively. When $P_s < P_c$ values of S_{f1}^* followed a similar trend with $N_t = A_z/A_h$ because they were primarily controlled by P_c . Conversely, when $P_s > P_c$ values of S_{f1}^* were also dependent on P_s . However, it should be mentioned that these trends also depended on the value of ζ_2 (data not shown). As discussed previously, the value of α_1^* follows similar trends as S_{f1}^* .

Figure 8 shows predicted values of α_2^* (Figure 8a) and S_{f2}^* (Figure 8b) with IS for $A_h = 500 \text{ nm}^2$, $\zeta_1 = -70 \text{ mV}$, $\zeta_2 = 20 \text{ mV}$, $P_s = 0.1$, $P_c = 0.57$, and $r_c = 5000, 2500, 1250, 500,$ and 250 nm . In contrast to Figure 6, the value of $\alpha_1^* = S_{f1}^*$ does not always equal zero in this situation. Comparison of Figures 6 and 8 reveals that α_2^* and S_{f2}^* exhibited similar behavior with IS and r_c . The main influence of chemical heterogeneity on the colloid and SWI was on the determination of S_{f1}^* (Figure 7), and this slightly influenced the calculated values of α_2^* and S_{f2}^* .

CONCLUSIONS

Charge heterogeneity on the surface of porous media and colloids is ubiquitous in natural environments, and has been widely recognized to influence colloid retention.^{3–17} However, previous attempts to account for charge heterogeneity by surface integration techniques have been applied at the scale of only a few micrometers because these approaches are computationally intensive.^{10,11,15,18–21} A simple modeling approach, that is consistent with findings from surface integration techniques, was presented herein to estimate colloid adhesive parameters on chemically heterogeneous surfaces at the REA scale which is much more relevant for predicting colloid transport and fate in the environment. Furthermore, this

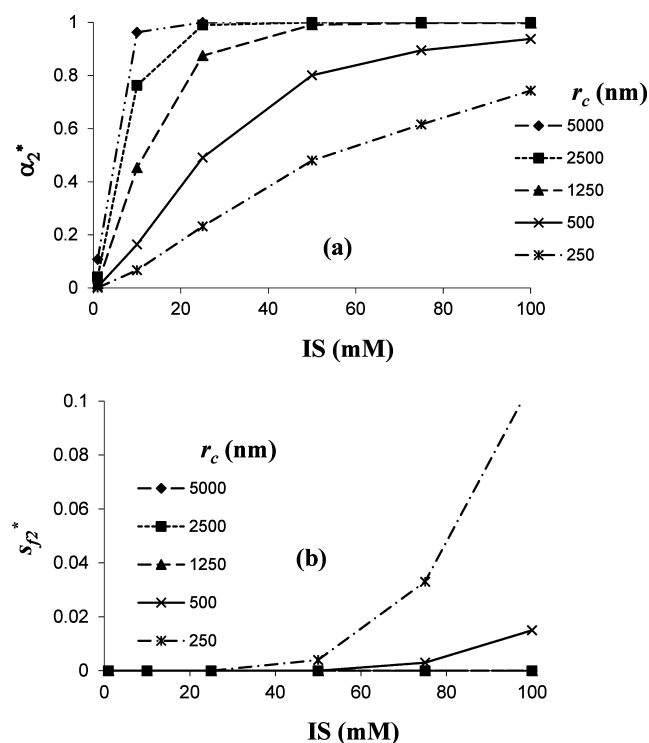


Figure 8. Predicted values of α^* (a) and S_f^* (b) as a function of IS for heterogeneously charged colloid and porous medium. Simulation properties included $A_h = 500 \text{ nm}^2$, $\zeta_1 = -70 \text{ mV}$ and $\zeta_2 = 20 \text{ mV}$ for both the colloid and the SWI, $P_c = 0.57$ to yield a mean ζ for the colloid equal to -30 mV to be consistent with Figure 6, $P_s = 0.1$, a Hamaker constant of $4.04 \times 10^{-21} \text{ J}$, and $r_c = 5000, 2500, 1250, 500$, and 250 nm .

approach is well suited to account for temporal variations in charge heterogeneity in natural environments because these calculations are executed rapidly.

Simulation results provide valuable insight on colloid adhesive parameters for chemically heterogeneous surfaces. For example, α^* and S_f^* were demonstrated to be very complex functions that depend on the charge heterogeneity properties (size, amount, and zeta potential), the colloid size, the solution chemistry, and the system hydrodynamics. In particular, irreversible colloid immobilization was predicted for smaller colloids and higher IS when $A_z \leq A_h$. Conversely, larger colloids and smaller IS tended to yield reversible interactions via a secondary minimum when $A_z > A_h$, and colloid immobilization could only be explained by consideration of other factors (e.g., surface roughness, eddy zones, and grain–grain contacts). Hysteresis in S_f^* with IS can occur because of the different dependence of reversible and irreversible colloid immobilization on solution chemistry. All these predictions are consistent with many incompletely understood experimental observations,^{27,48–59,63–66} and therefore, the modeling approach provides a powerful tool to help interpret data.

AUTHOR INFORMATION

Corresponding Author

*Phone: 951-369-4857. E-mail: Scott.Bradford@ars.usda.gov.

Notes

The authors declare no competing financial interest.

ACKNOWLEDGMENTS

We would like to acknowledge helpful discussion with Ranoj Duffadar. This research was supported by the USDA, ARS, NP 214. The USDA is an equal opportunity provider and employer.

REFERENCES

- (1) Derjaguin, B. V.; Landau, L. D. Theory of the stability of strongly charged lyophobic sols and of the adhesion of strongly charged particles in solutions of electrolytes. *Acta Physicochim. U.S.S.R.* **1941**, *14*, 733–762.
- (2) Verwey, E. J. W.; Overbeek, J. Th. G. *Theory of the stability of lyophobic colloids*; Elsevier: Amsterdam, 1948.
- (3) Foppen, J. W. A.; Schijven, J. F. Evaluation of data from the literature on the transport and survival of *Escherichia coli* and thermotolerant coliforms in aquifers under saturated conditions. *Water Res.* **2006**, *40*, 401–426.
- (4) Kim, S.-B.; Park, S.-J.; Lee, C.-G.; Kim, H.-C. Transport and retention of *Escherichia coli* in a mixture of quartz, Al-coated and Fe-coated sands. *Hydrol. Processes* **2008**, *22*, 3856–3863.
- (5) Metge, D. W.; Harvey, R. W.; Aiken, G. R.; Anders, R.; Lincoln, G.; Jasperse, J. Influence of organic carbon loading, sediment associated metal oxide content and sediment grain size distributions upon *Cryptosporidium parvum* removal during riverbank filtration operations, Sonoma County, CA. *Water Res.* **2010**, *44*, 1126–1137.
- (6) Abudalo, R. A.; Bogatsu, Y. G.; Ryan, J. N.; Harvey, R. W.; Metge, D. W.; Elimelech, M. Effect of ferric oxyhydroxide grain coatings on the transport of bacteriophage PRD1 and *Cryptosporidium parvum* oocysts in saturated porous media. *Environ. Sci. Technol.* **2005**, *39*, 6412–6419.
- (7) Attinti, R.; Wei, J.; Kniel, K.; Sims, J. T.; Jin, Y. Virus' (MS2, ϕ X174, and Aichi) attachment on sand measured by atomic force microscopy and their transport through sand columns. *Environ. Sci. Technol.* **2010**, *44*, 2426–2432.
- (8) Syngouna, V. I.; Chrysikopoulos, C. V. Interaction between viruses and clays in static and dynamic batch systems. *Environ. Sci. Technol.* **2010**, *44*, 4539–4544.
- (9) Suresh, L.; Walz, J. Y. Effect of surface roughness on the interaction energy between a colloidal sphere and a flat plate. *J. Colloid Interface Sci.* **1996**, *183*, 199–213.
- (10) Bhattacharjee, S.; Ko, C.-H.; Elimelech, M. DLVO interaction between rough surfaces. *Langmuir* **1998**, *14*, 3365–3375.
- (11) Hoek, E. M. V.; Agarwal, G. K. Extended DLVO interactions between spherical particles and rough surfaces. *J. Colloid Interface Sci.* **2006**, *298*, 50–58.
- (12) Kozlova, N.; Santore, M. M. Manipulation of micrometer-scale adhesion by tuning nanometer-scale surface features. *Langmuir* **2006**, *22*, 1135–1142.
- (13) Duffadar, R. D.; Davis, J. M. Interaction of micrometer-scale particles with nanotextured surfaces in shear flow. *J. Colloid Interface Sci.* **2007**, *308*, 20–29.
- (14) Santore, M. M.; Kozlova, N. Micrometer scale adhesion on nanometer-scale patchy surfaces: Adhesion rates, adhesion thresholds, and curvature-based selectivity. *Langmuir* **2007**, *23*, 4782–4791.
- (15) Duffadar, R. D.; Davis, J. M. Dynamic adhesion behavior of micrometer-scale particles flowing over patchy surfaces with nanoscale electrostatic heterogeneity. *J. Colloid Interface Sci.* **2008**, *326*, 18–27.
- (16) Kalasin, S.; Santore, M. M. Hydrodynamic crossover in dynamic microparticle adhesion on surfaces of controlled nanoscale heterogeneity. *Langmuir* **2008**, *24*, 4435–4438.
- (17) Duffadar, R. D.; Kalasin, S.; Davis, J. M.; Santore, M. M. The impact of nanoscale chemical features on micron-scale adhesion: Crossover from heterogeneity-dominated to mean-field behavior. *J. Colloid Interface Sci.* **2009**, *337*, 396–407.
- (18) Bhattacharjee, S.; Elimelech, M. Surface element integration: A novel technique for evaluation of DLVO interaction between a particle and a flat plate. *J. Colloid Interface Sci.* **1997**, *193*, 273–285.

- (19) Hoek, E. M. V.; Bhattacharjee, S.; Elimelech, M. Effect of membrane surface roughness on colloid-membrane DLVO interactions. *Langmuir* **2003**, *19*, 4836–4847.
- (20) Martines, E.; Csaderova, L.; Morgan, H.; Curtis, A. S. G.; Riehle, M. O. DLVO interaction energy between a sphere and a nano-patterned plate. *Colloids Surf., A* **2008**, *318*, 45–52.
- (21) Bendersky, M.; Davis, J. M. DLVO interaction of colloidal particles with topographically and chemically heterogeneous surfaces. *J. Colloid Interface Sci.* **2011**, *353*, 87–97.
- (22) Ma, H. L.; Pazmino, E.; Johnson, W. P. Surface heterogeneity on hemispheres-in-cell model yields all experimentally-observed non-straining colloid retention mechanisms in porous media in the presence of energy barriers. *Langmuir* **2011**, *27*, 14982–14994.
- (23) Harvey, R. W.; Garabedian, S. P. Use of colloid filtration theory in modeling movement of bacteria through a contaminated sandy aquifer. *Environ. Sci. Technol.* **1991**, *25*, 178–185.
- (24) Sun, N.; Elimelech, M.; Sun, N.-Z.; Ryan, J. N. A novel two-dimensional model for colloid transport in physically and geochemically heterogeneous porous media. *J. Contam. Hydrol.* **2001**, *49*, 173–199.
- (25) Schijven, J. F.; Simunek, J. Kinetic modeling of virus transport at the field scale. *J. Contam. Hydrol.* **2002**, *55*, 113–135.
- (26) Grolimund, D.; Borkovec, M. Release of colloidal particles in natural porous media by monovalent and divalent cations. *J. Contamin. Hydrol.* **2006**, *87*, 155–175.
- (27) Bradford, S. A.; Torkzaban, S.; Kim, H.; Simunek, J. Modeling colloid and microorganism transport and release with transients in solution ionic strength. *Water Resour. Res.* **2012**, *48*, W09509.
- (28) Yao, K.-M.; Habibian, M. T.; O'Melia, C. R. Water and waste water filtration: Concepts and applications. *Environ. Sci. Technol.* **1971**, *5*, 1105–1112.
- (29) Adamczyk, Z.; Siwek, B.; Zembala, M.; Belouschek, P. Kinetics of localized adsorption of colloid particles. *Adv. Colloid Interface Sci.* **1994**, *48*, 151–280.
- (30) Hogg, R.; Healy, T. W.; Fuerstenau, D. W. Mutual coagulation of colloidal dispersions. *Trans. Faraday Soc.* **1966**, *62*, 1638–1651.
- (31) Gregory, J. Approximate expression for retarded van der Waals interaction. *J. Colloid Interface Sci.* **1981**, *83*, 138–145.
- (32) Bergendahl, J.; Grasso, D. Colloid generation during batch leaching tests: mechanics of disaggregation. *Colloids Surf., A* **1998**, *135*, 193–205.
- (33) Israelachvili, J. N. *Intermolecular and surface forces*; Academic Press: San Diego, CA, 1992.
- (34) Bergendahl, J.; Grasso, D. Prediction of colloid detachment in a model porous media: hydrodynamics. *Chem. Eng. Sci.* **2000**, *55*, 1523–1532.
- (35) Das, S. K.; Schechter, R. S.; Sharma, M. M. The role of surface roughness and contact deformation on the hydrodynamic detachment of particles from surfaces. *J. Colloid Interface Sci.* **1994**, *164*, 63. I.
- (36) Johnson, K. L.; Kendall, K.; Roberts, A. D. Surface energy and the contact of elastic solids. *Proc. R. Soc. London. Ser. A* **1971**, *324*, 301–313.
- (37) Maugis, D. Adhesion of spheres: The JKR-DMT transition using a dugdale model. *J. Colloid Interface Sci.* **1992**, *150*, 243–269.
- (38) Bradford, S. A.; Torkzaban, S.; Walker, S. L. Coupling of physical and chemical mechanisms of colloid straining in saturated porous media. *Water Res.* **2007**, *41*, 3012–3024.
- (39) Torkzaban, S.; Bradford, S. A.; Walker, S. L. Resolving the coupled effects of hydrodynamics and DLVO forces on colloid attachment to porous media. *Langmuir* **2007**, *23*, 9652–9660.
- (40) Torkzaban, S.; Tazehkand, S. S.; Walker, S. L.; Bradford, S. A. Transport and fate of bacteria in porous media: Coupled effects of chemical conditions and pore space geometry. *Water Resour. Res.* **2008**, *44*, W04403.
- (41) Shen, C.; Huang, Y.; Li, B.; Jin, Y. Predicting attachment efficiency of colloid deposition under unfavorable attachment conditions. *Water Resour. Res.* **2010**, *46*, W11526.
- (42) Bradford, S. A.; Torkzaban, S.; Wiegmann, A. Pore-scale simulations to determine the applied hydrodynamic torque and colloid immobilization. *Vadose Zone J.* **2011**, *10*, 252–261.
- (43) Bradford, S. A.; Kim, H. N.; Haznedaroglu, B. Z.; Torkzaban, S.; Walker, S. L. Coupled factors influencing concentration-dependent colloid transport and retention in saturated porous media. *Environ. Sci. Technol.* **2009**, *43*, 6996–7002.
- (44) Simoni, S. F.; Harms, H.; Bosma, T. N. P.; Zehnder, A. J. B. Population heterogeneity affects transport of bacteria through sand columns at low flow rates. *Environ. Sci. Technol.* **1998**, *32*, 2100–2105.
- (45) Dong, H.; Onstott, T. C.; Ko, C.-H.; Hollingsworth, A. D.; Brown, D. G.; Mailloux, B. J. Theoretical prediction of collision efficiency between adhesion-deficient bacteria and sediment grain surface. *Colloids Surf., B* **2002**, *24*, 229–245.
- (46) Shen, C.; Li, B.; Huang, Y.; Jin, Y. Kinetics of coupled primary and secondary-minimum deposition of colloids under unfavorable chemical conditions. *Environ. Sci. Technol.* **2007**, *41*, 6976–6982.
- (47) Jury, W. A.; Roth, K. *Transfer functions and solute movement through soils: Theory and applications*; Birkhauser Verlag: Basel, Switzerland, 1990.
- (48) Johnson, P. R.; Sun, N.; Elimelech, M. Colloid transport in geochemically heterogeneous porous media: modeling and measurements. *Environ. Sci. Technol.* **1996**, *30*, 3284–3293.
- (49) Torkzaban, S.; Kim, Y.; Mulvihill, M.; Wan, J.; Tokunaga, T. K. Transport and deposition of functionalized CdTe nanoparticles in saturated porous media. *J. Contamin. Hydrol.* **2010**, *118*, 208–217.
- (50) Elimelech, M.; Nagai, M.; Ko, C. H.; Ryan, J. N. Relative insignificance of mineral grain zeta potential to colloid transport in geochemically heterogeneous porous media. *Environ. Sci. Technol.* **2000**, *34*, 2143–2148.
- (51) Wang, Y.; Li, Y.; Fortner, J. D.; Hughes, J. B.; Abriola, L. M.; Pennell, K. D. Transport and retention of nanoscale C60 aggregates in water-saturated porous media. *Environ. Sci. Technol.* **2008**, *42*, 3588–3594.
- (52) Bradford, S. A.; Torkzaban, S.; Simunek, J. Modeling colloid transport and retention in saturated porous media under unfavorable attachment conditions. *Water Resour. Res.* **2011**, *47*, W10503.
- (53) Wang, D.; Bradford, S. A.; Paradelo, M.; Peijnenburg, W. J. G. M.; Zhou, D. Facilitated Transport of Cu with hydroxyapatite nanoparticles in saturated sand: Effects of velocity, pH, and iron oxide grain coating. *Soil Sci. Soc. Am. J.* **2012**, *76*, 375–388.
- (54) Johnson, W. P.; Li, X.; Assemi, S. Deposition and re-entrainment dynamics of microbes and non-biological colloids during non-perturbed transport in porous media in the presence of an energy barrier to deposition. *Adv. Water Resour.* **2007**, *30*, 1432–1454.
- (55) Bradford, S. A.; Simunek, J.; Bettahar, M.; Tadassa, Y. F.; van Genuchten, M. T.; Yates, S. R. Straining of colloids at textural interfaces. *Water Resour. Res.* **2005**, *41*, W10404.
- (56) Bradford, S. A.; Simunek, J.; Walker, S. L. Transport and straining of *E. coli* O157:H7 in saturated porous media. *Water Resour. Res.* **2006**, *42*, W12S12.
- (57) Choi, N.-C.; Kim, D.-J.; Kim, S.-B. Quantification of bacterial mass recovery as a function of pore-water velocity and ionic strength. *Res. Microbiol.* **2007**, *158*, 70–78.
- (58) Tong, M.; Ma, H.; Johnson, W. P. Funneling of flow into grain-to-grain contacts drives colloid–colloid aggregation in the presence of an energy barrier. *Environ. Sci. Technol.* **2008**, *42*, 2826–2832.
- (59) Shen, C.; Huang, Y.; Li, B.; Jin, Y. Effects of solution chemistry on straining of colloids in porous media under unfavorable conditions. *Water Resour. Res.* **2008**, *44*, W05419 DOI: 10.1029/2007WR006580.
- (60) Vaidyanathan, R.; Tien, C. Hydrosol deposition on granular beds. *Chem. Eng. Sci.* **1988**, *43*, 289–302.
- (61) Taneda, S. Visualization of separating Stokes flows. *J. Phys. Soc. Jpn.* **1979**, *46*, 1935–1942.
- (62) Li, X.; Li, Z.; Zhang, D. Role of low flow and backward flow zones on colloid transport in pore structures derived from real porous media. *Environ. Sci. Technol.* **2010**, *44*, 4936–4942.
- (63) Torkzaban, S.; Kim, H. N.; Simunek, J.; Bradford, S. A. Hysteresis of colloid retention and release in saturated porous media

during transients in solution chemistry. *Environ. Sci. Technol.* **2010**, *44*, 1662–1669.

(64) Bradford, S. A.; Kim, H. Causes and implications of colloid and microorganism retention hysteresis. *J. Contamin. Hydrol.* **2012**, *138–139*, 83–92.

(65) Bradford, S. A.; Kim, H. Implications of cation exchange on clay release and colloid-facilitated transport in porous media. *J. Environ. Qual.* **2010**, *39*, 2040–2046.

(66) Shen, C.; Lazouskaya, V.; Jin, Y.; Li, B.; Zheng, W.; Ma, Z.; Huang, Y. Coupled factors influencing detachment of nano- and micro-sized particles from primary minima. *J. Contamin. Hydrol.* **2012**, *134–135*, 1–11.